A&A 433, 717–730 (2005)
DOI: 10.1051/0004-6361:20041771

Astronomy & Astrophysics

Atomic data from the IRON Project

LVIII. Electron impact excitation of Fe XII⋆

P. J. Storey[1], G. Del Zanna[2], H. E. Mason[2], and C. J. Zeippen[3]

[1] Department of Physics and Astronomy, University College London, Gower Street, London WC1E 6BT, UK
e-mail: PJS@star.ucl.ac.uk
[2] Department of Applied Mathematics and Theoretical Physics, Centre for Mathematical Sciences, Wilberforce Road, Cambridge CB3 0WA, UK
[3] UMR 8102 (associée au CNRS et à l'Université Paris 7) et LUTH, Observatoire de Paris, 92195 Meudon, France

Received 2 August 2004 / Accepted 1 November 2004

Abstract. A new calculation of rate coefficients for electron collisional excitation of Fe XII is presented and compared to earlier calculations. Significant differences are found with all earlier work due to the inclusion of resonance processes that have not previously been considered and to the use of the intermediate coupling frame transformation method. The resulting dataset of collision strengths is shown to resolve many of the outstanding discrepancies between theory and solar observations. In particular, density sensitive line ratios in Fe XII now indicate electron densities close to those derived from other ions of comparable ionization potential.

Key words. atomic data – Sun: corona – techniques: spectroscopic

1. Introduction

Spectroscopic diagnostics using UV, EUV and X-ray emission line intensities are a fundamental tool for the measurement of physical parameters of solar plasma, such as electron density, temperature, emission measure and chemical composition. These diagnostics require a large amount of accurate atomic data, including radiative and collisional transition probabilities. Fe plays a key role in diagnostic studies because of its wealth of strong spectral lines covering a wide wavelength range. Fe XII is a particularly important ion, since it exists at a temperature ($T_e = 1.5 \times 10^6$ K) typical of the coronal plasma. Although the Fe XII coronal lines have been observed for over three decades (from early 1970's rocket flights to the recent Solar nad Heliospheric Observatory, SOHO, observations), their intensities have remained one of the outstanding puzzles in the analysis of solar spectra. Substantial inconsistencies between the electron densities derived from Fe XII and other coronal ions have led to serious doubts about the reliability of available Fe XII atomic data. This has provided a major challenge for atomic physicists, which can only now be solved with the development of sophisticated atomic physics codes and the availability of sufficient computing resources and time. This current work has been carried out as part of the international IRON Project (Hummer et al. 1993; a complete list of published papers and those in press is available on-line[1]). The IRON project aims to provide accurate atomic data for all the astrophysically interesting iron ions.

Flower (1977), was the first to carry out ab initio atomic calculations (radiative data and electron impact data) for Fe XII. He provided distorted-wave (DW) collision strengths between the ground configuration $3s^23p^3$ and the first two excited configurations $3s3p^4$ and $3s^23p^23d$. Further atomic data (radiative data and electron impact excitation data obtained with the *R*-matrix close coupling codes) was provided for the $3s^23p^3$ to $3s3p^4$ configurations by Tayal et al. (1987) and Tayal & Henry (1988). However, serious deficiencies in these results were pointed out by Mason (1994). Further R-matrix calculations were carried out as part of the IRON Project by Binello et al. (1998a, 1998b, hereafter referred to as B98a and B98b). These authors provided new electron impact excitation data for the three lowest configurations using an extensive basis set to describe the target. At that time this was a state-of-the-art calculation which pushed the limits of computing power. A detailed comparison of the theoretical intensities obtained for Fe XII with the available solar spectra, from the *Solar EUV Rocket Telescope and Spectrograph* (SERTS), was carried out by Binello et al. (2001). This showed up continuing significant inconsistencies between the theoretical and the observed

⋆ Table 10 is only available in electronic form at the CDS via anonymous ftp to cdsarc.u-strasbg.fr (130.79.128.5) or via http://cdsweb.u-strasbg.fr/cgi-bin/qcat?J/A+A/433/717

[1] http://www.usm.uni-muenchen.de/people/ip/iron-project.html

data which could not be fully explained, except by the assumption that many of the Fe XII lines were blended. A detailed discussion was given in Binello et al. (2001) of all previous calculations for Fe XII and also all available solar observations. These details will not be repeated here. In the summary and conclusions of Binello et al. (2001) it was proposed that a yet more elaborate target and calculation of electron excitation data might be needed. This has now been carried out in the current study. Lines from Fe XII have been recorded by many solar missions (e.g. Skylab, SOHO, SERTS) and will be of particular importance for future missions such as the Solar-B, EUV Imaging Spectrometer.

This paper focuses on the atomic calculations, described in Sect. 2. The results in terms of collision strengths are compared with previous calculations in Sect. 3, while Sect. 4 compares the spectral line intensities of a few important transitions with a selected set of observations. Conclusions are presented in Sect. 5. A follow-up paper (Del Zanna & Mason 2005) will deal with the issue of line identifications and with further extensive comparisons with observations.

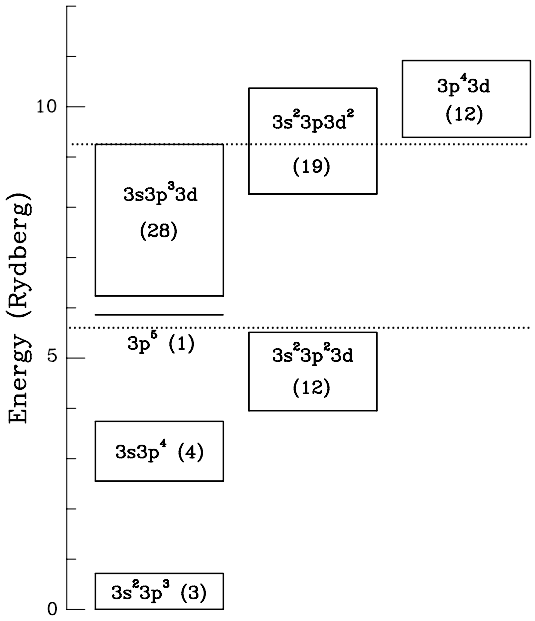

Fig. 1. The energetically lowest electron configurations of Fe XII. Numbers in parentheses indicate the number of terms in that configuration.

2. Atomic data

2.1. Background

This paper is the fourth in a series of papers describing calculations of transition probabilities and collision strengths for electron impact excitation of Fe XII. The first two of the earlier papers dealt with excitation of the fine-structure transitions in the ground configuration of Fe XII (B98a) and the excitation of optically allowed and intercombination transitions of Fe XII (B98b). The third paper discussed possible shortcomings in the excitation rates reported in the first two papers and attempted to address one of these shortcomings, the omission of excitation by cascade mechanisms (Binello et al. 2001). We refer readers to this latter paper for a fuller description of theoretical work on electron excitation of Fe XII prior to that of B98a.

In this section, we outline the perceived shortcomings in B98a and B98b and report the results of an extended calculation of electron impact excitation of Fe XII designed to overcome these problems.

In Fig. 1 we show the distribution of the energetically lowest electron configurations of Fe XII. Transitions between the $3s3p^4$ and $3s^23p^23d$ configurations and the ground $3s^23p^3$ give rise to the observed spectral lines in the far UV. The lower dotted line in Fig. 1 shows the upper limit of the scattering target used in B98a and B98b, which included 19 terms. Since that calculation was made, the importance of particular higher configurations, in this case the $3s3p^33d$ configuration, has become clearer. Binello et al. (2001) discussed the importance of excitation of the UV lines by cascade processes, noting that the three higher lying odd parity configurations, $3p^5$, $3s3p^33d$ and $3s^23p3d^2$ are connected by electric dipole radiative decays to the two even parity configurations which give rise to the UV lines. These three configurations can be populated by electron excitation from the ground configuration, although the process is expected to be relatively weak as there is no dipole coupling. The process of population by excitation and radiative cascade may, nonetheless, be significant for those states for which direct electron excitation from the ground terms is inefficient.

Binello et al. (2001) tested the importance of this effect by extending the earlier work (B98a, B98b) to generate a scattering target that included all the terms of the $3p^5$ and $3s3p^33d$ configurations and some from the $3s^23p3d^2$ configuration, giving a total of 58 target terms. They then computed collision strengths at one energy above all the target states with a partial wave expansion that extended to electron orbital angular momentum $l = 19$. From these approximate collision strengths, collision rates were computed to the terms of the additional configurations that were used to supplement the data from the earlier calculations (B98a, B98b) and the UV line intensities were compared to observation. Only small changes were found in the theoretical line intensities (Binello et al. 2001).

The approximate treatment used by Binello et al. (2001) was incomplete in two ways. Firstly, no allowance was made for the energy variation of the collision strengths for the additional target states and in addition, the partial wave expansion was truncated. Secondly, computing collision strengths at only one energy above all thresholds ignores the fact that the additional target configurations give rise to resonances that affect the collision rates for transitions between the lower terms, including those in the original 19-state calculation. This effect has been shown to be very important for Fe XIV by Storey et al. (2000) and for Fe IX by Storey & Zeippen (2001) and Storey et al. (2002). In the latter case, collision strengths for transitions between some metastable states in Fe IX are increased by factors of between 4 and 14 (Storey et al. 2002) when the resonances converging to the equivalent electron configurations are added to the Fe IX target.

Table 1. The target configuration basis and orbital scaling parameters.

Configurations		Scaling parameters†	
$3s^2\,3p^3$	$3s\,3p^4$	1s	1.41337
$3p^5$		2s	1.11538
$3s\,3p^3\,3d$	$3s^2\,3p^2\,3d$	3s	1.13461
	$3p^4\,3d$	2p	1.06220
$3s^2\,3p\,3d^2$	$3s\,3p^2\,3d^2$	3p	1.10992
$3p^3\,3d^2$		3d	1.13567
$3s\,3p\,3d^3$	$3s^2\,3d^3$		
	$3p^2\,3d^3$		

† See text for physical significance of the scaling parameters.

2.2. The scattering target

The configuration basis describing the target for the present calculation is shown in Table 1. For the scattering calculation the lowest 58 *LS* terms are included which give rise to 143 levels. As stated above the target includes all states belonging to the five energetically lowest electron configurations plus 28 levels of the $3s^23p3d^2$ configuration. Ideally, the whole $3s^23p3d^2$ configuration would be included. In practice, including the whole configuration would also involve including most of a further configuration ($3p^43d$, see Fig. 1), significantly enlarging the size of the scattering problem. Also, the two new configurations, $3s3p^33d$ and $3s^23p3d^2$ differ in that the first is accessible from the ground configuration by a single electron 3s–3d transition, while the second requires a two-electron $3s^2$–$3d^2$ transition which is expected to be weaker, leading to a weaker cascade process. The target extent is illustrated by the upper dotted line in Fig. 1. A full list of the 58 target terms is given in Table 2, and shows the theoretical values and the experimental values where they are known. The target wave functions were calculated with the general purpose atomic structure code SUPERSTRUCTURE (Eissner et al. 1974; Nussbaumer & Storey 1978), and the scaling parameters for the statistical model potentials in which the orbital functions are calculated are also given in Table 1. The calculation of the target wave functions is carried out in LS-coupling, but with the one-body mass and Darwin relativistic energy shifts included. Incorporating these shifts leads to better agreement between the calculated and experimental energies, without the greatly increased computational cost of carrying out the scattering calculation including fine-structure interactions. This procedure was discussed and the effects illustrated for scattering from Ca^{7+} by Saraph & Storey (1996). The theoretical energies quoted in Table 2 were calculated in this way except for those in italics, which have been empirically corrected as described in B98a, using the experimental data available for the higher terms of the $3s^23p^23d$ configuration. We note that the target configuration basis, and therefore the derived energies and also the target oscillator strengths are the same as those obtained by B98a. The target oscillator strengths for the strongest optically allowed transitions were given in *LS* coupling in Table 2 of B98a, described as "set 2".

In Table 3 we show the energies of the first 41 of the target levels. The column headed E_{SS} contains the energies obtained

Table 2. Energies of target terms in Rydberg.

Term		Exp.†	Calculated
$3s^23p^3$	$^4S^o$	0.	0.
	$^2D^o$	0.4035	0.4295
	$^2P^o$	0.7142	0.6821
$3s3p^4$	^4P	2.5507	2.5329
	^2D	3.1067	3.1056
	^2P	3.5651	3.6035
	^2S	3.7398	3.6993
$3s^23p^23d$	^4F		*3.9137*
	^2F		*4.0324*
	^4D		*4.0813*
	^2G		*4.4976*
	^2P	4.6093	4.6741
	^4P	4.6942	4.7694
	^2D	4.8595	4.9128
	^2D	5.0519	5.1223
	^2S	5.2295	5.3257
	^2P	5.2380	5.3351
	^2F	5.2788	5.3891
	^2D	5.5091	5.5787
$3s3p^33d$	$^6D^o$		5.7084
$3p^5$	$^2P^o$		5.8423
$3s3p^33d$	$^4D^o$		6.2280
	$^4F^o$		6.3491
	$^2S^o$		6.6214
	$^4G^o$		6.7068
	$^2G^o$		6.9676
	$^4P^o$		7.0190
	$^4D^o$		7.0624
	$^2D^o$		7.0800
	$^4F^o$		7.1436
	$^4P^o$		7.2349
	$^4S^o$		7.2386
	$^2F^o$		7.2765
	$^2D^o$		7.4408
	$^4D^o$		7.4716
	$^2P^o$		7.5050
	$^2F^o$		7.6001
	$^2G^o$		7.6635
	$^4D^o$		7.9305
	$^2D^o$		7.9566
	$^2P^o$		8.0429
	$^2F^o$		8.0497
	$^2D^o$		8.2433
$3s^23p3d^2$	$^4G^o$		8.2463
	$^2S^o$		8.2523
$3s3p^33d$	$^2F^o$		8.3319
	$^2P^o$		8.3425
$3s^23p3d^2$	$^4D^o$		8.6891
$3s3p^33d$	$^2P^o$		8.7640
$3s^23p3d^2$	$^2F^o$		8.7914
	$^4F^o$		8.8107
	$^4P^o$		8.8315
	$^2H^o$		8.8966
	$^2D^o$		8.9159
	$^2G^o$		9.0283
$3s3p^33d$	$^2D^o$		9.1475
$3s^23p3d^2$	$^4D^o$		9.2174
$3s3p^33d$	$^2S^o$		9.2262

† Jupen et al. (1993); Corliss & Sugar (1982).

Table 3. Fine-structure energies (cm^{-1}) from the scattering target E_{SS}, with the adjusted SS values E_{emp} and the experimental energies E_{exp}.

i	Conf.	Term	E_{emp}	E_{SS}	$E^{\dagger}_{exp}$
1	$3s^2\ 3p^3$	$^4S^o_{3/2}$	0	0	0
2	$3s^2\ 3p^3$	$^2D^o_{3/2}$		44 401	41 555
3	$3s^2\ 3p^3$	$^2D^o_{5/2}$		48 820	46 088
4	$3s^2\ 3p^3$	$^2P^o_{1/2}$		76 629	74 108
5	$3s^2\ 3p^3$	$^2P^o_{3/2}$		82 567	80 515
6	$3s\ 3p^4$	$^4P^e_{5/2}$		273 532	274 373
7	$3s\ 3p^4$	$^4P^e_{3/2}$		282 792	284 005
8	$3s\ 3p^4$	$^4P^e_{1/2}$		287 061	288 307
9	$3s\ 3p^4$	$^2D^e_{3/2}$		341 572	339 761
10	$3s\ 3p^4$	$^2D^e_{5/2}$		343 371	341 703
11	$3s\ 3p^4$	$^2P^e_{3/2}$		394 054	389 668
12	$3s\ 3p^4$	$^2P^e_{1/2}$		398 658	394 598
13	$3s\ 3p^4$	$^2S^e_{1/2}$		413 990	410 401
14	$3s^2\ 3p^2\ 3d$	$^4F^e_{3/2}$	424 352	432 916	
15	$3s^2\ 3p^2\ 3d$	$^4F^e_{5/2}$	428 068	436 626	
16	$3s^2\ 3p^2\ 3d$	$^4F^e_{7/2}$	433 506	442 078	
17	$3s^2\ 3p^2\ 3d$	$^2F^e_{5/2}$	438 499	449 368	
18	$3s^2\ 3p^2\ 3d$	$^4F^e_{9/2}$	440 301	448 928	
19	$3s^2\ 3p^2\ 3d$	$^2F^e_{7/2}$	443 231	453 150	
20	$3s^2\ 3p^2\ 3d$	$^4D^e_{1/2}$	444 296	452 295	
21	$3s^2\ 3p^2\ 3d$	$^4D^e_{3/2}$	445 395	453 437	
22	$3s^2\ 3p^2\ 3d$	$^4D^e_{5/2}$	449 330	458 091	
23	$3s^2\ 3p^2\ 3d$	$^4D^e_{7/2}$	457 991	467 678	
24	$3s^2\ 3p^2\ 3d$	$^2G^e_{7/2}$	493 123	503 892	
25	$3s^2\ 3p^2\ 3d$	$^2G^e_{9/2}$	496 132	506 852	
26	$3s^2\ 3p^2\ 3d$	$^2P^e_{3/2}$		510 206	501 800
27	$3s^2\ 3p^2\ 3d$	$^4P^e_{5/2}$		521 694	512 510
28	$3s^2\ 3p^2\ 3d$	$^2P^e_{1/2}$		521 853	513 850
29	$3s^2\ 3p^2\ 3d$	$^4P^e_{3/2}$		525 619	516 740
30	$3s^2\ 3p^2\ 3d$	$^4P^e_{1/2}$		528 117	519 770
31	$3s^2\ 3p^2\ 3d$	$^2D^e_{3/2}$		535 550	526 120
32	$3s^2\ 3p^2\ 3d$	$^2D^e_{5/2}$		546 510	538 040
33	$3s^2\ 3p^2\ 3d$	$^2D^e_{3/2}$		563 827	554 030
34	$3s^2\ 3p^2\ 3d$	$^2D^e_{5/2}$		564 733	554 610
35	$3s^2\ 3p^2\ 3d$	$^2P^e_{1/2}$		582 557	568 940
36	$3s^2\ 3p^2\ 3d$	$^2F^e_{5/2}$		589 243	576 740
37	$3s^2\ 3p^2\ 3d$	$^2P^e_{3/2}$		590 534	577 740
38	$3s^2\ 3p^2\ 3d$	$^2S^e_{1/2}$		588 805	579 630
39	$3s^2\ 3p^2\ 3d$	$^2F^e_{7/2}$		593 625	581 180
40	$3s^2\ 3p^2\ 3d$	$^2D^e_{5/2}$		616 414	603 930
41	$3s^2\ 3p^2\ 3d$	$^2D^e_{3/2}$		617 981	605 480

† Jupen et al. (1993); Corliss & Sugar (1982).

using the 12 configuration basis of the scattering calculation, including the spin-orbit interaction but not the two-body relativistic interactions. This is the approximation used in the calculation of the so-called term-coupling coefficients used in the scattering calculation. Since the interaction between levels of the same J and parity depends, to a first approximation, on the inverse of the energy difference between them, it is instructive to compare the calculated separations of strongly interacting levels with the observed ones. We return to this point when we compare collision strengths and effective collision strengths with earlier work in subsequent sections.

The energies of four of the terms of the $3s^23p^23d$ configuration are not known experimentally. In the column headed E_{emp} we give adjusted theoretical energies for these levels, obtained by applying empirical corrections to the calculated energies E_{SS}. The corrections are calculated from the difference between theory and observation for other terms of the same configuration and the same parentage whose energies are experimentally known. Note that this procedure results in different estimates for these energies to those given in B98a.

2.3. The scattering calculation

The R-matrix method used in this calculation is described elsewhere (Hummer et al. 1993, and references therein). As outlined above, we include mass and Darwin relativistic energy shifts, but not the one- and two-body fine-structure interactions. We use an R-matrix boundary radius of 3.09 au, to encompass the most extended target orbital (3d). The expansion of each scattered electron partial wave is over a basis of 20 functions within the R-matrix boundary, and the partial wave expansion extends to a maximum total orbital angular momentum quantum number of $L = 18$. The outer region calculation is carried out using the intermediate-coupling frame transformation method (ICFT) described by Griffin et al. (1998), in which the transformation to intermediate coupling uses the so-called term-coupling coefficients (TCCs), and is complete up to a total angular momentum quantum number, $J = 15$. We have supplemented this calculation, which includes exchange, with a non-exchange calculation that extends from $J = 16$ to $J = 50$. Dipole-allowed transitions are also topped-up to infinite partial wave using an intermediate coupling version of the Coulomb-Bethe method as described by Burgess (1974) while non-dipole allowed transitions were topped-up assuming that the collision strengths form a geometric progression in J for $J > 50$. Once all collision strengths have been corrected for missing angular momenta, they are extrapolated to energies higher than 100 Ryd using techniques and asymptotic expressions discussed by Burgess & Tully (1992). We shall refer to this calculation as ICFT58.

3. Comparisons

3.1. Comparisons of the collision strengths

3.1.1. The transitions within the ground configuration

In Fig. 2 we compare collision strengths from the present calculation (ICFT58) with B98a for three transitions among levels of the ground $3s^23p^3$ configuration. The plots cover the energy region where some channels are closed and many resonances are present. The collision strengths have been averaged over 0.5 Ryd intervals so that the magnitude of the resonance contributions can be more easily seen. For the two transitions from level 1 ($3s^23p^3\ ^4S^o_{3/2}$), the present results are substantially larger than those of B98a. At first glance this is an unexpected

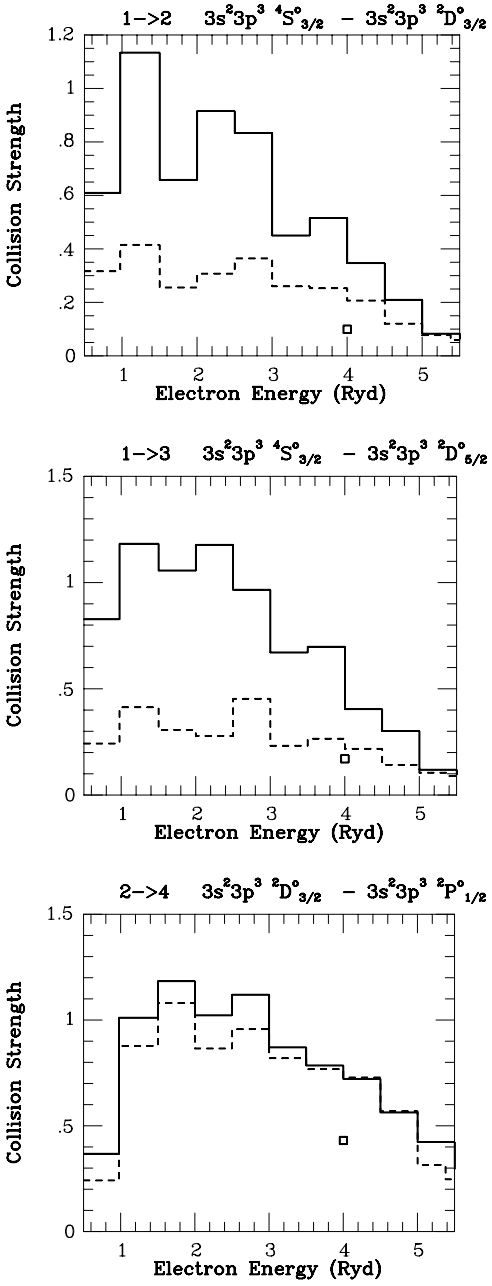

Fig. 2. Collision strengths in the resonance region, averaged over 0.5 Ryd intervals, for three transitions within the ground configuration. Solid line – present work (ICFT58). Dashed line – Binello et al. (1998a). Squares – Tayal & Henry (1988).

result for two reasons: 1) the target basis in the present work and that of Binello et al. (1998a) is the same; and 2) the resonance contributions to these two transitions arise primarily from series converging on the $3s3p^4$ and to a lesser extent the $3s^23p^23d$ configurations, which were fully included in the target in both calculations. However, there are two differences between the two calculations. The present calculation has 58 target terms while that of B98a had only 19 terms and in addition the present work used the ICFT method described by Griffin et al. (1998) while B98a transformed to intermediate coupling using the technique described by Saraph (1978).

In order to illustrate the effect of this latter change, we have carried out two further calculations, using only the 19-term target of B98a. In the first, which we shall call ICFT19, we have used exactly the same target and basis as B98a but carried out the outer region calculation using the ICFT method. In the second (BP19), we have again used the same basis as B98a but carried out a full Breit-Pauli calculation with a target containing the 41-levels that arise from the 19 LS-terms. In the Breit-Pauli calculation all spin-orbit fine-structure interactions are included in the target and in the scattering calculation explicitly. The calculation included total angular momenta $0 \leq J \leq 10$ and was not corrected for contributions from higher J. It is therefore reliable for the forbidden transitions among the levels of the ground configuration but not for permitted transitions where higher partial wave contributions are expected to be important. This calculation is also computationally much more demanding, and could not be carried out for our full target but is expected to give the most accurate results in the resonance region.

In Fig. 3 we compare the results of these two additional calculations with those of Binello et al. (1998a) for the same three transitions. There is excellent agreement between ICFT19 and BP19 but significant disagreement with B98a. Comparing corresponding figures in Figs. 2 and 3 shows that there is also good agreement between ICFT19, BP19 and the results of the full 58-state target calculation. These figures show that, for the forbidden transitions within the ground configuration, the ICFT method gives results that agree closely with a full Breit-Pauli calculation and also agree reasonably well with the results using a larger target. It is apparent that, for transitions from the ground level, significant resonance contributions were omitted in the work of B98a due to the method used rather than any approximation in the target. The most likely cause of the difference lies in the way that the term-coupling coefficients are used in the two calculations. In the ICFT method, where non-physical matrices are used it is possible to transform channels from LS to intermediate coupling using term-coupling coefficients even when the channels are closed. Thus, for the energy region between the $3s^23p^3$ and $3s3p^4$ configurations where there are resonances converging on the terms of the $3s3p^4$ configuration, it is possible to incorporate the fine-structure interactions between quartet and doublet target terms in a way that is impossible using the method of Saraph (1978). Mixing between levels of doublet and quartet terms of the $3s3p^4$ configuration means that collision strengths between the $^4S^o_{3/2}$ level and the doublet levels of the ground configuration can be enhanced by resonances converging on the quartet terms of the $3s3p^4$ configuration. In the method of Saraph (1978) this mixing can only be incorporated at energies where the channels are open, not in the resonance region. In the paper describing the ICFT method, Griffin et al. (1998) have demonstrated and discussed these effects for a small model calculation. In this paper we show that they persist for larger calculations and have significant spectroscopic consequences.

It is also worth noting that since entire Rydberg series of resonances are introduced by using the ICFT method, uncertainties in the positions of near threshold resonances have little effect on the rate coefficients derived from these cross-sections.

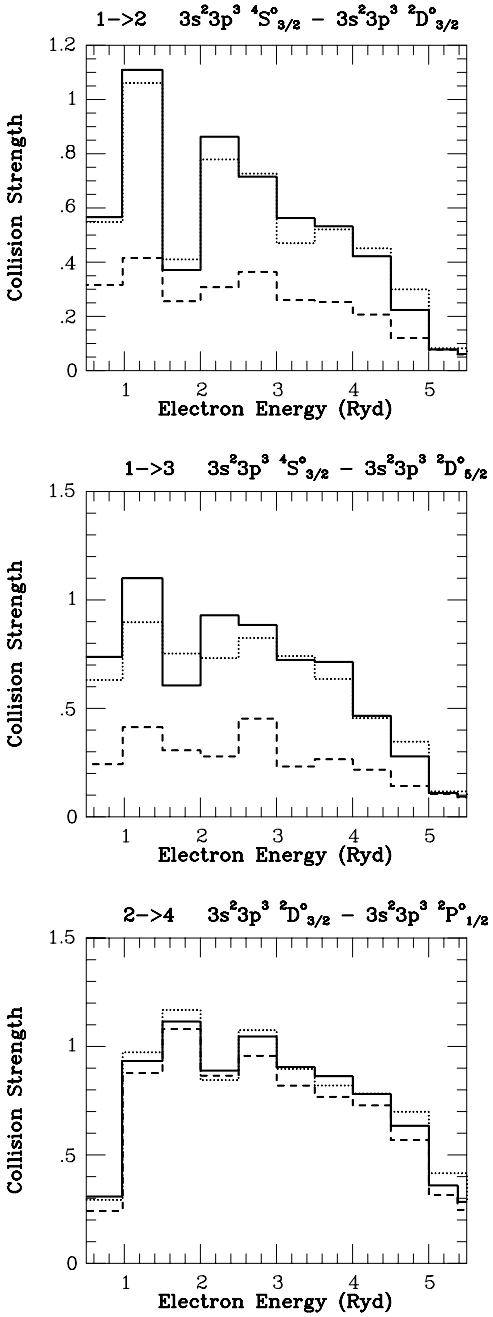

Fig. 3. Collision strengths in the resonance region, averaged over 0.5 Ryd intervals, for three transitions within the ground configuration. Solid line – present work, Breit-Pauli approximation BP19. Dotted line – present work, ICFT19. Dashed line – Binello et al. (1998a).

3.1.2. Transitions to the $3s3p^4$ and $3s^23p^23d$ configurations

In Fig. 4 we compare the present results with those of B98a and B98b for four transitions from the ground level $3s^23p^3\ {}^4S^o_{3/2}$ to the $3s3p^4$ and $3s^3p^23d$ configurations. In the first three cases ($1 \rightarrow 6, 1 \rightarrow 10, 5 \rightarrow 10$), the new results are significantly larger, particularly for the relatively weak spin-changing transition $3s^23p^3\ {}^4S^o_{3/2}$–$3s3p^4\ {}^2D^o_{5/2}$. The enhancements are due to resonances converging upon the states of the $3s3p^33d$

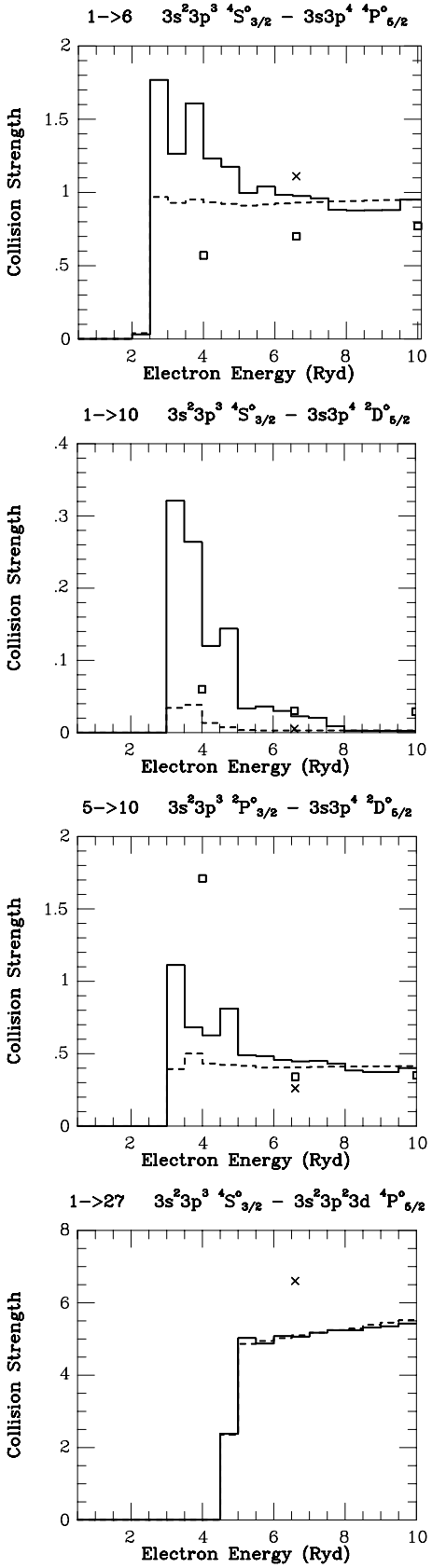

Fig. 4. Collision strengths for four transitions from the ground configuration, $3s^23p^3$, to the configurations $3s3p^4$ and $3s^23p^23d$. The collision strengths are averaged over 0.5 Ryd intervals. Solid line – present work, ICFT58. Dashed line – Binello et al. (1998a). Squares – Tayal & Henry (1988). Crosses – Flower (1977).

configuration which are included as target states in the present 58-state calculation but not in the smaller 19-state target of B98a and B98b. Many transitions between the $3s3p^4$ and $3s3p^23d$ configurations are dipole allowed, leading to large resonance contributions which strongly enhance the intrinsically weak transitions such as $3s^23p^3\ ^4S^o_{3/2}$–$3s3p^4\ ^2D^o_{5/2}$.

The fourth transition in Fig. 4, $3s^23p^3\ ^4S^o_{3/2}$–$3s^23p^23d\ ^4P_{5/2}$, shows very close agreement between the two sets of results. The collision strengths for the other strong dipole transitions between these two configurations are also in good agreement.

3.2. Comparisons of thermally averaged collision strengths

In Tables 4 and 5 we compare thermally averaged collision strengths obtained with the present 58-state calculation with those of B98a and B98b at two temperatures. As expected from the comparison of collision strengths, the largest differences are seen for transitions from the ground level to other levels of the ground configuration and for the lower temperature, where low-lying resonances have the greatest effect on the thermal average. Significant increases in effective collision strengths are also present for some of the other transitions to the higher configurations. This can also be seen in Figs. 5 and 6 which compares our results with those of B98a and B98b and Tayal et al. (1987).

The significant increase in excitation rates from the ground level to the other four levels of the ground configuration leads to a significantly higher population of these four levels compared to those obtained with the results of B98a and B98b or with any previous calculation. This point and its consequences will be discussed further below. There is generally very good agreement with B98a and B98b at high temperature where the thermal average is determined by the high energy behaviour of the collision strength which is expected to be the same.

3.3. Level populations

The radiative data (transition probabilities A_{ji} from the upper level j to the lower level i) have been calculated using SUPERSTRUCTURE in the twelve configuration basis shown in Table 1, and, to maintain consistency with the scattering calculation, including the spin-orbit interaction but not two-body relativistic interactions. The transition probabilities are published solely in electronic form, as Table 10. A more elaborate calculations of transition probabilities among the lowest three electron configurations was published by B98a (their Basis 3A results). A further detailed study of A-values using the configuration expansion of B98a including two-body relativistic terms and semi-empirical corrections to the transition energies has been published by Del Zanna & Mason (2005). The equations of statistical equilibrium have been solved to obtain $N_j(N_e, T_e)$, the fractional population of level j relative to the total number density of the ion, as a function of the electron temperature and number density.

Additionally, proton excitations and photo-excitations can be important processes for the forbidden transitions taking place between levels within the same configuration. However, the addition of these two processes only slightly affect the level balance, and the intensities of the lines considered here. For

Table 4. Effective collision strengths for transitions $3s^2\ 3p^3$–$3s^2\ 3p^3$ and $3s^2\ 3p^3$–$3s\ 3p^4$, calculated at two temperatures, and compared with the results from Binello et al. (1998a, B98).

Log T	5.60	5.60	6.15	6.15
i–j	this work	B98	this work	B98
1–2	0.6070	0.2683	0.2909	0.1431
1–3	0.7883	0.2679	0.3825	0.1582
1–4	0.1969	0.0741	0.0877	0.0386
1–5	0.4039	0.3044	0.1803	0.1503
1–6	1.2830	0.8614	1.1220	0.9898
1–7	0.8107	0.5652	0.7198	0.6445
1–8	0.4176	0.2837	0.3657	0.3238
1–9	0.1229	0.0049	0.0459	0.0037
1–10	0.1416	0.0045	0.0515	0.0032
1–11	0.1548	0.0771	0.0847	0.0587
1–12	0.0717	0.0264	0.0351	0.0201
1–13	0.0470	0.0124	0.0220	0.0109
2–3	2.0170	2.3750	0.9602	1.1840
2–4	0.8310	0.7629	0.5328	0.5067
2–5	1.0160	1.4180	0.5688	0.8001
2–6	0.2227	0.0457	0.1001	0.0351
2–7	0.1833	0.0331	0.0759	0.0213
2–8	0.1018	0.0163	0.0407	0.0106
2–9	1.1010	0.8267	1.0780	1.0110
2–10	0.2850	0.0844	0.1303	0.0609
2–11	0.3299	0.1869	0.2428	0.1946
2–12	0.6374	0.5174	0.6485	0.6204
2–13	0.1117	0.0463	0.0622	0.0429
3–4	0.6488	0.5554	0.4049	0.3657
3–5	1.8840	1.7790	1.2110	1.1620
3–6	0.3940	0.0824	0.1758	0.0643
3–7	0.2417	0.0305	0.0955	0.0191
3–8	0.0960	0.0092	0.0354	0.0045
3–9	0.3243	0.1041	0.1498	0.0724
3–10	1.6840	1.1570	1.5050	1.3540
3–11	1.5310	1.2540	1.5260	1.4670
3–12	0.1109	0.0247	0.0438	0.0131
3–13	0.0891	0.0191	0.0341	0.0097
4–5	1.0900	1.2410	0.5359	0.6634
4–6	0.0893	0.0149	0.0356	0.0079
4–7	0.0894	0.0213	0.0387	0.0141
4–8	0.0505	0.0170	0.0260	0.0145
4–9	0.2428	0.1308	0.1777	0.1396
4–10	0.1523	0.0535	0.0675	0.0323
4–11	0.1673	0.0932	0.1253	0.1010
4–12	0.4113	0.3362	0.4224	0.4175
4–13	0.1400	0.0742	0.1088	0.0883
5–6	0.2407	0.0480	0.1007	0.0302
5–7	0.1622	0.0440	0.0761	0.0331
5–8	0.0819	0.0222	0.0359	0.0141
5–9	0.2277	0.0719	0.1023	0.0463
5–10	0.6913	0.3843	0.5261	0.4293
5–11	0.3221	0.1752	0.2381	0.1925
5–12	0.1312	0.0377	0.0507	0.0166
5–13	0.8410	0.7153	0.8548	0.8333

Table 5. Effective collision strengths for transitions $3s^2\ 3p^3$–$3s^2\ 3p^2\ 3d$, calculated at two temperatures, and compared with the results from Binello et al. (1998a, B98).

Log T	5.60	5.60	6.15	6.15
i–j	this work	B98	this work	B98
1–14	0.1149	0.0470	0.0610	0.0364
1–15	0.1509	0.0684	0.0841	0.0531
1–16	0.1808	0.0854	0.1004	0.0643
1–17	0.1080	0.1111	0.0514	0.0826
1–18	0.2122	0.0378	0.1218	0.0381
1–19	0.1656	0.0082	0.0647	0.0061
1–20	0.0586	0.0265	0.0236	0.0170
1–21	0.1198	0.0258	0.0572	0.0251
1–22	0.1603	0.0280	0.0797	0.0240
1–23	0.1216	0.0217	0.0486	0.0143
1–24	0.0129	0.0012	0.0047	0.0006
1–25	0.0114	0.0016	0.0041	0.0005
1–26	0.0368	0.0172	0.0254	0.0171
1–27	5.1560	5.1850	5.8270	5.9350
1–28	0.0749	0.0550	0.0797	0.0649
1–29	3.4390	3.4660	3.8910	3.9630
1–30	1.7120	1.7320	1.9360	1.9810
1–31	0.1284	0.1213	0.1384	0.1355
1–32	0.1342	0.1253	0.1445	0.1403
1–33	0.0047	0.0011	0.0021	0.0007
1–34	0.0120	0.0051	0.0084	0.0057
1–35	0.0071	0.0012	0.0048	0.0008
1–36	0.0377	0.0304	0.0312	0.0282
1–37	0.0133	0.0045	0.0084	0.0036
1–38	0.0032	0.0074	0.0016	0.0058
1–39	0.0343	0.0285	0.0238	0.0216
1–40	0.0259	0.0220	0.0229	0.0212
1–41	0.0095	0.0073	0.0067	0.0059

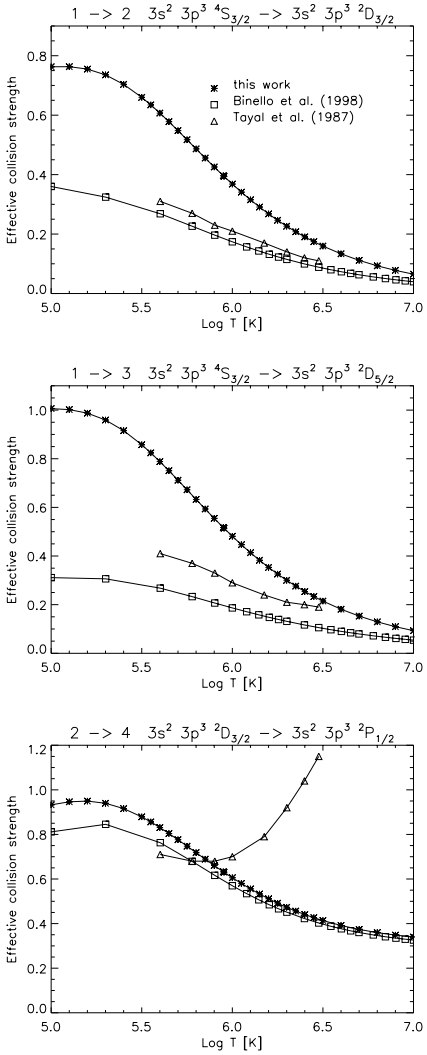

Fig. 5. Effective collision strengths for a sample of transitions within the ground $3s^2\ 3p^3$ configuration, compared with previous calculations.

completeness, the proton excitation rates of Landman (1978) have been included in the calculations.

The fractional populations of the levels of the ground configuration and the most populated higher levels is given in Table 6 at three values of the electron density. In Table 7 we compare the fractional populations of the levels of the ground configuration with those obtained from the atomic data of F77 and B98a,b. Effective collision strengths were obtained from the collision strength data given at one energy of 6.6 Ryd in F77 using the scaling methods described by Burgess & Tully (1992). For energies below 6.6 Ryd we assume all collision strengths to have their value at 6.6 Ryd and at higher energies we interpolate linearly to the high energy limit as described by Burgess & Tully (1992).

Comparing our results first with those obtained from the B98a,b data, the fraction of the population residing in the four levels of the $^2D^o$ and $^2P^o$ terms is considerably larger in the present work. This is due to the increase in the collision strengths for direct excitation from the ground level due to resonance processes as described in Sect. 3. In the present work, and in the results from B98a,b, about half the population of the levels of the $^2D^o$ and $^2P^o$ terms arises from direct excitation and cascade within the ground configuration itself. These processes are more effective in the present work, whereas cascading from higher states is of comparable magnitude in the two calculations.

As shown in Table 7, however, the populations derived from the F77 data are larger than those derived from B98a,b even though the F77 collision strengths among the levels of the ground configuration are much smaller than those of B98a,b. The higher populations derived from the F77 dataset arise principally from cascades from just two levels of the $3s^23p^23d$ configuration, $^2P_{1/2}$ (level 28) and $^2D_{3/2}$ (level 31). In the present work the effective collision strengths to these two levels from the ground level are 0.080 and 0.138 respectively at $\log T = 6.15$ (see Table 5) whereas from F77, the equivalent values are 0.79 and 0.54. The relatively large collisions strengths to these two levels arise from spin-orbit interactions with the ^4P levels of the same J value. These interactions are much smaller in the present work compared to the results of F77. The magnitude of the interaction depends, to a first approximation, on the inverse of the energy separation between the two states involved. In the F77 calculation these separations are underestimated compared to experiment, leading to

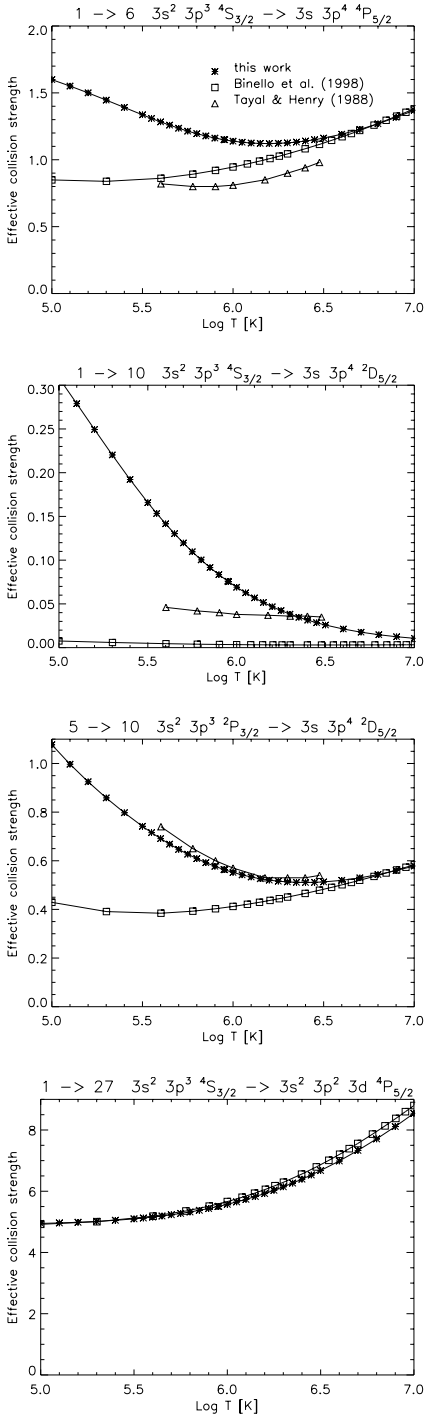

Fig. 6. Effective collision strengths for a sample of $3s^2\ 3p^3$–$3s\ 3p^4$ and $3s^2\ 3p^3$–$3s^2\ 3p^2\ 3d$ transitions, compared with the previous calculations of Binello et al. (1998a).

an overestimate of the collision strengths. For example, the energy separation between the $^4P_{1/2}$ and $^2P_{1/2}$ levels (levels 30 and 28) is observed to be 5920 cm^{-1}, whereas F77 calculated 3985 cm^{-1} and in the present calculation we find 6264 cm^{-1}. The good agreement between our calculated separation and experiment gives us confidence that the magnitude of the interaction between these levels is accurately calculated in the present work and therefore that the derived collision strengths are reliable. A similar result is found for the $^4P_{3/2}$ and $^2D_{3/2}$ levels.

Table 6. Fractional level population N_j of the most populated levels, calculated at different densities (cm^{-3}) and at Log T[K] = 6.15.

i	10^8	10^{10}	10^{12}
1	0.94	0.58	0.29
2	4.0×10^{-3}	0.13	0.18
3	5.3×10^{-2}	0.25	0.31
4	1.1×10^{-4}	1.6×10^{-2}	6.6×10^{-2}
5	1.0×10^{-4}	1.8×10^{-2}	0.13
15	1.7×10^{-10}	1.3×10^{-8}	1.1×10^{-6}
16	1.0×10^{-9}	8.8×10^{-8}	6.8×10^{-6}
17	1.3×10^{-10}	2.1×10^{-8}	2.8×10^{-6}
18	2.3×10^{-4}	9.6×10^{-3}	1.3×10^{-2}
19	5.2×10^{-10}	7.5×10^{-8}	8.5×10^{-6}
23	5.4×10^{-8}	6.7×10^{-6}	7.1×10^{-4}
25	6.0×10^{-6}	1.8×10^{-3}	8.7×10^{-3}

Table 7. Fractional level population N_j of the levels of the ground configuration, calculated at 10^8 cm^{-3} and Log T[K] = 6.15, and compared with the values we calculated from the Flower (1977, F77) and Binello et al. (1998a, B98) data. Note the significant increase in the population of the ^{2}D and ^{2}P levels.

		This work	F77	B98
1	$^4S^o_{3/2}$	0.94	0.97	0.97
2	$^2D^o_{3/2}$	4.0×10^{-3}	3.7×10^{-3}	2.5×10^{-3}
3	$^2D^o_{5/2}$	5.3×10^{-2}	3.0×10^{-2}	2.7×10^{-2}
4	$^2P^o_{1/2}$	1.1×10^{-4}	7.7×10^{-5}	5.7×10^{-5}
5	$^2P^o_{3/2}$	1.0×10^{-4}	6.8×10^{-5}	7.4×10^{-5}

4. Line intensities: Comparisons with observations

Given the level population densities, N_j, we can calculate the theoretical line intensities. Rather than providing tables of calculated and observed line ratios (for the cases approximately independent of the electron density), and tables of densities derived from observed line ratios, we follow the method described in Del Zanna et al. (2004) in which we plot the ratios, F_{ji}, between theoretical and observed, ($I_{\rm ob}$), line intensities (scaled by the electron density $N_{\rm e}$):

$$F_{ji} = \frac{I_{\rm ob} N_{\rm e}}{N_j(N_{\rm e}, T_0)\, A_{ji}}, \qquad (1)$$

calculated at a fixed temperature T_0, as a function of the electron density $N_{\rm e}$. If agreement between theory and observations is exact, all the F_{ji} curves will either overlap or cross at one density value (the averaged electron density). The F_{ji} absolute value of the crossing would depend on a proportionality constant which depends on the elemental abundance, the ion fraction, the geometry of the emission, and the units of the observed intensities. In what follows, the F_{ji} curves of each dataset have been normalized to an arbitrary value, and calculated at

Table 8. Some of the brightest/most important Fe XII spectral lines in the EUV, discussed in this paper. The A_{ji} values calculated here, and those calculated by Binello et al. (2001, B01) are shown.

i–j	λ (Å)	Transition	A_{ji}	A_{ji} (B01)
2–36	186.854 (bl)	$^2D^o_{3/2}$–$^2F^e_{5/2}$	1.0×10^{11}	1.0×10^{11}
3–39	186.887 (bl)	$^2D^o_{5/2}$–$^2F^e_{7/2}$	1.1×10^{11}	1.1×10^{11}
1–30	192.394	$^4S^o_{3/2}$–$^4P^e_{1/2}$	9.0×10^{10}	8.8×10^{10}
1–29	193.509	$^4S^o_{3/2}$–$^4P^e_{3/2}$	9.0×10^{10}	8.9×10^{10}
1–27	195.119 (bl)	$^4S^o_{3/2}$–$^4P^e_{5/2}$	8.8×10^{10}	8.6×10^{10}
2–33	195.179 (bl)	$^2D^o_{3/2}$–$^2D^e_{3/2}$	6.0×10^{10}	5.7×10^{10}
3–34	196.640 (bl Fe XIII)	$^2D^o_{5/2}$–$^2D^e_{5/2}$	4.5×10^{10}	4.1×10^{10}
3–10	338.264	$^2D^o_{5/2}$–$^2D^e_{5/2}$	2.8×10^{9}	2.8×10^{9}
1–8	346.852	$^4S^o_{3/2}$–$^4P^e_{1/2}$	1.8×10^{9}	1.8×10^{9}
1–7	352.106	$^4S^o_{3/2}$–$^4P^e_{3/2}$	1.7×10^{9}	1.7×10^{9}
1–6	364.467	$^4S^o_{3/2}$–$^4P^e_{5/2}$	1.6×10^{9}	1.6×10^{9}

log T_0 [K] = 6.15, the temperature of peak abundance of Fe^{11+} in ionization equilibrium. Note that, for the combinations of lines presented, the choice of T_0 is negligible compared to the theoretical and experimental uncertainties.

A plot of F_{ji} curves has the advantage of giving a global view of all the lines at once, and clearly shows which lines are best for calibration or as a density diagnostic.

4.1. Experimental data

We restrict our discussion to the brightest EUV Fe XII lines, observed in the 180–200 and 330–370 Å spectral ranges (see Table 8), important for electron density diagnostics and instrument calibration.

In order to assess the accuracy of the atomic data we require observations with high spectral resolution and with a radiometric calibration. Very few sets of solar observations meet these requirements.

A general overview of the problem of benchmarking atomic calculations against experimental data can be found in Del Zanna et al. (2004), while more details concerning Fe XII are given in Del Zanna & Mason (2005). In what follows we briefly describe the datasets that we have selected.

Behring et al. (1976) have presented a whole-Sun spectrum with excellent resolution (0.06 Å), covering the 160–770 Å range. Although Behring et al. (1976) only provided indicative intensities, all the groups of lines discussed here are close in wavelength, and considering the instrumentation used, large calibration effects are not expected.

Malinovsky & Heroux (1973) presented an integrated-Sun spectrum covering the 50–300 Å range with a medium resolution (0.25 Å), taken with a grazing-incidence spectrometer flown on a rocket in 1969. The spectrum was photometrically calibrated (uncertainties in the relative radiometric calibration are ∼10% for lines close in wavelength), and still represent the best available spectrum in the EUV 150–300 Å range, for lines that are not blended.

The Goddard Solar Extreme Ultraviolet Rocket Telescope and Spectrograph (SERTS) has been flown several times since 1989, and has produced data of excellent spectral resolution. The SERTS-89 (Thomas & Neupert 1994) data covered the 170–225 Å range in second order and the 235–450 Å range in first order. The SERTS-89 data were radiometrically calibrated on the ground against primary standards and in theory could be used for the benchmark. However, Young et al. (1998), when performing a detailed benchmark of CHIANTI atomic data on the SERTS-89 spectrum, found major inconsistencies (by factors of 2) in the calibration of the second order lines and of the 400–450 Å region. We have therefore chosen to use here only the first order.

The SERTS-95 spectra (Brosius et al. 1998b) covered the 171–225 Å band in second-order, and the 235–335 Å region in first order with excellent spectral resolution (*FWHM* = 0.03, 0.05 Å respectively). The SERTS-95 calibration needs revision, since it was based on old atomic data for several ions (CHIANTI version 1.01, see Brosius et al. 1998a).

4.2. Comparisons

The brightest Fe XII lines are found in the EUV, in the 180–200 Å range (see Table 8). Note that, in most medium-resolution spectra, many of these lines are blended. This is one of the reasons why we also use high-resolution data, even if the calibration is more uncertain. The F_{ji} curves relative to the above-mentioned observations are shown in Figs. 7–10.

4.2.1. Density-insensitive line groups

The decays from the $3s^23p^23d\ ^4P^e_{1/2,3/2,5/2}$ levels to the ground state (transitions 1–27, 1–29, 1–30) are predicted by theory to have approximately constant ratios, independent of electron density. Our results are in excellent agreement with observations, as shown in Figs. 7 (top) and 8 (top). On the other hand, a significant disagreement with observation is found with the use of the Flower (1977) collision strengths, as shown in Figs. 7 (bottom) and 8 (bottom). This disagreement, already noted by previous authors (e.g. Zhitnik et al. 1998), is present in many other cases. As noted by Binello et al. (1998b), there are many transitions for which Flower (1977) largely under- or over-estimated the collision strengths. This was ultimately

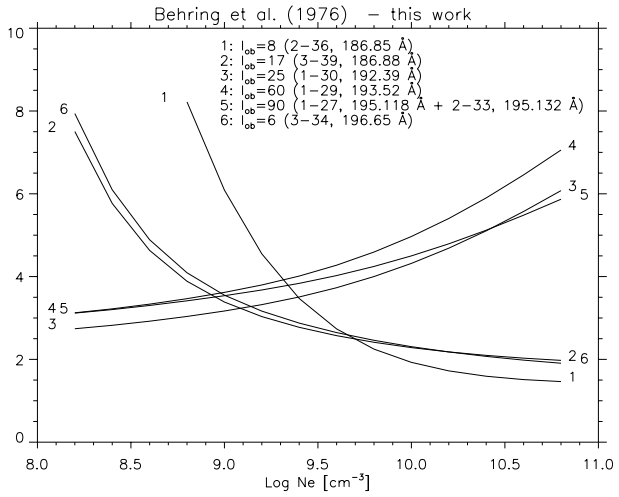

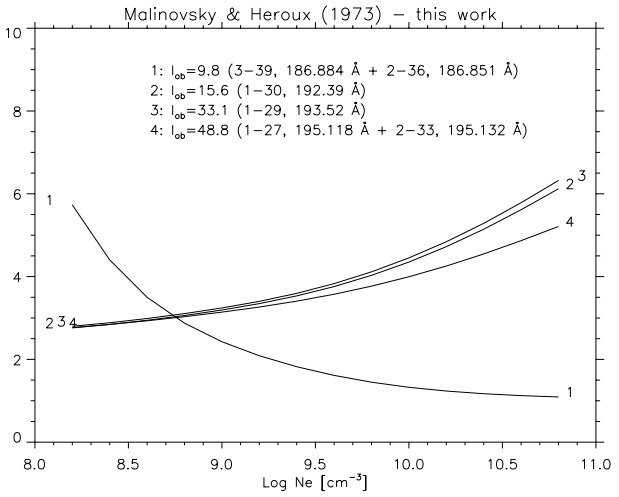

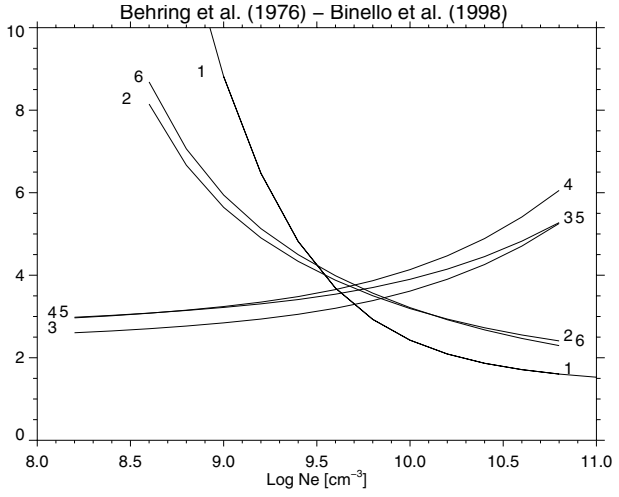

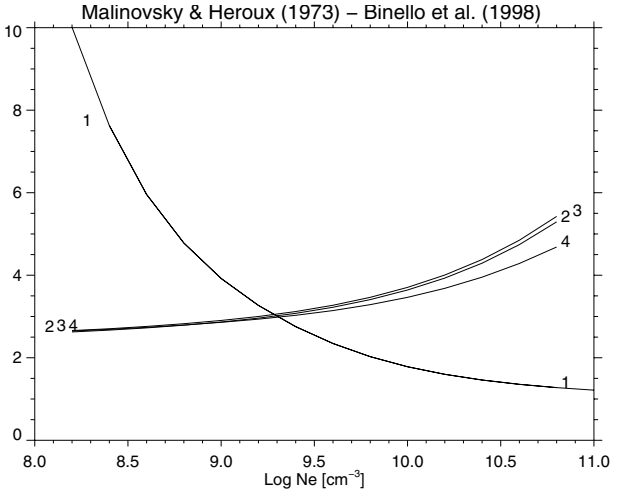

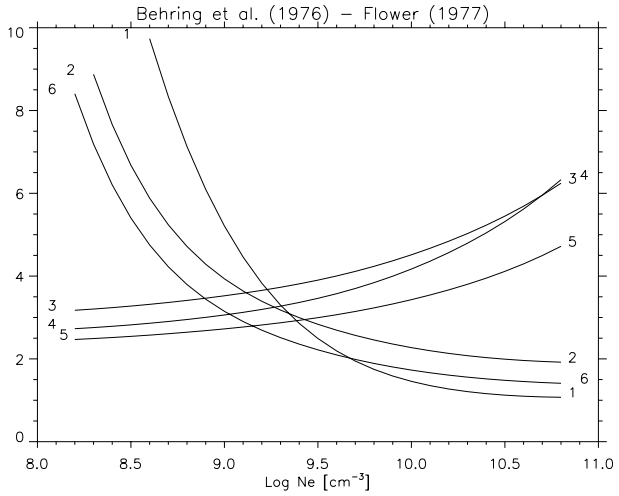

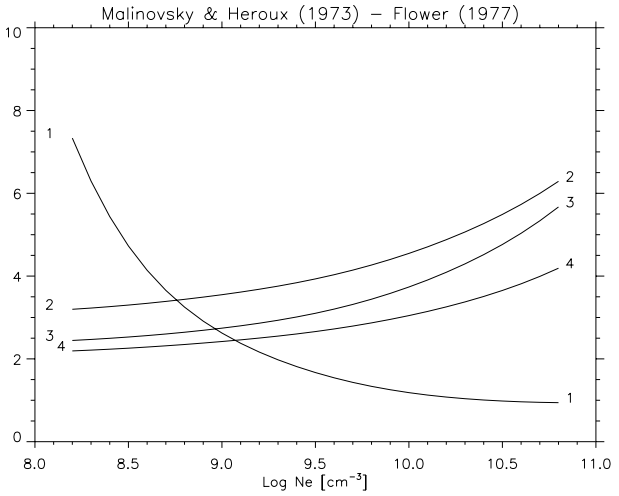

Fig. 7. The F_{ji} curves of the Behring et al. (1976) whole Sun observations, using different atomic data.

Fig. 8. The F_{ji} curves relative to the full-Sun spectrum of Malinovsky & Heroux (1973). The agreement between our present model and the observations is excellent. The curves also indicate an electron density $\log N_e = 8.8$ cm^{-3}, in excellent agreement with the values derived from other ions.

related to the simple scattering approximation (distorted wave) and limited target used by Flower (1977). Note that the results of Binello et al. (1998a,b) are also in good agreement with observations, as shown in Figs. 7 (centre) and 8 (centre).

A similar argument applies to the transitions from the $3s3p^4\ ^4P^e_{1/2,3/2,5/2}$ levels (transitions 1–6, 1–7, 1–8), as shown in Figs. 9, 10. The calibrated spectra of Thomas & Neupert (1994) show an excellent correspondence between our predicted intensities and the observed intensities.

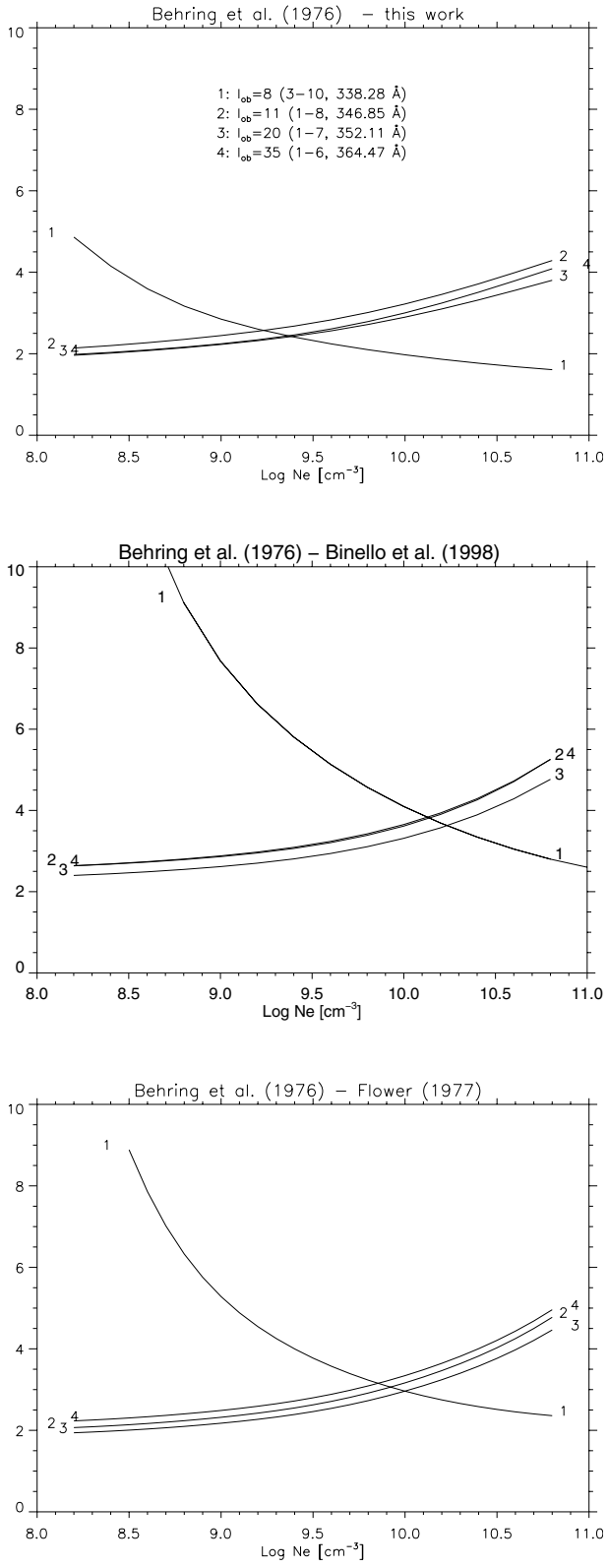

Fig. 9. The F_{ji} curves of the Behring et al. (1976) whole Sun observations, using different atomic data.

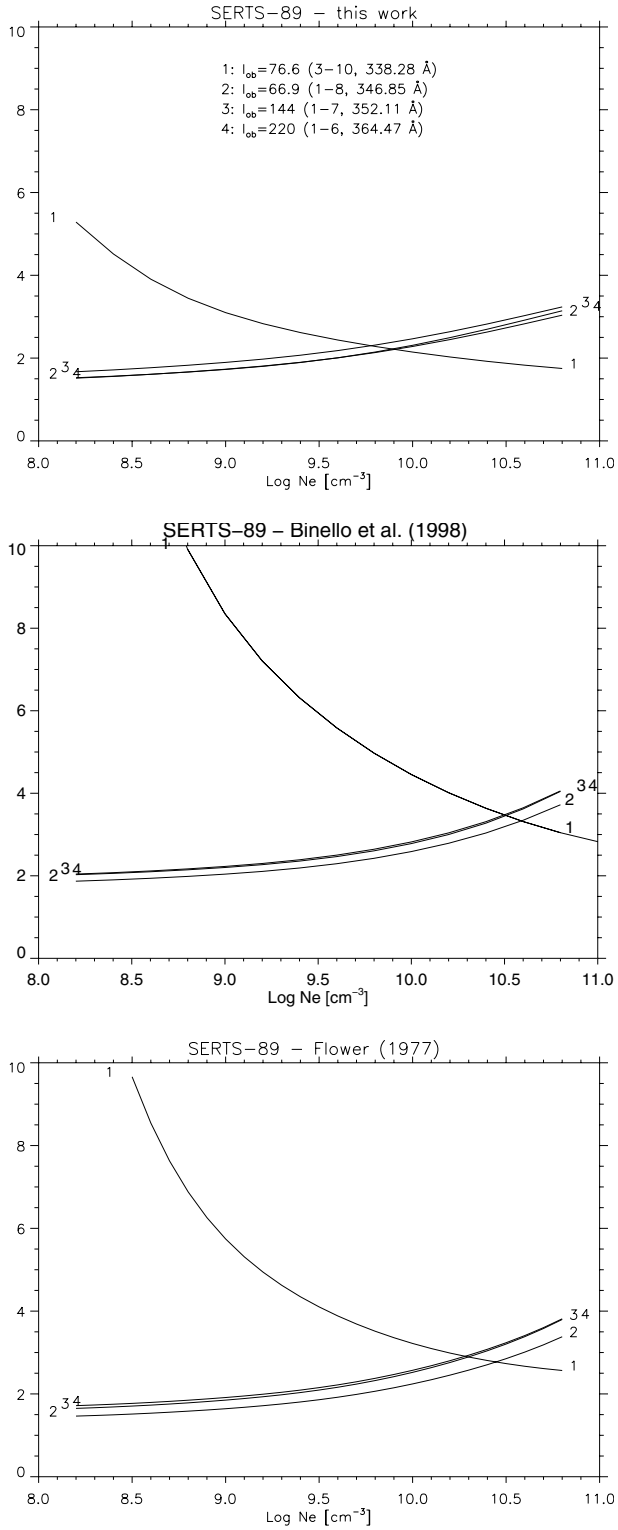

Fig. 10. F_{ji} curves relative to the averaged active region spectrum of SERTS-89 (Thomas & Neupert 1994), using different atomic data.

4.2.2. Density-sensitive line groups

The 2–36 (186.854 Å), 3–39 (186.887 Å), 3–34 (196.640 Å), and 3–10 (338.264 Å) lines provide excellent density diagnostics for the solar corona. In most solar spectra, the 3–39 (186.887 Å) transition is self-blended (at all electron densities) with the 2–36 (186.854 Å) Fe XII line, while the bright 3–34 (196.640 Å) transition is blended with an Fe XIII line at 196.54 Å.

However, in the high-resolution spectra of Behring et al. (1976), these lines are resolved (note that the authors

Table 9. Electron densities (log values, in cm^{-1}) derived from density sensitive line ratios and from the SERTS-95 active region (AR) and quiet-Sun (QS) spectra.

Ratio (λ in Å)	SERTS-95 AR			SERTS-95 QS		
	F77	B01	Present work	F77	B01	Present work
186.87/192.39	$10.0^{+0.2}_{-0.2}$	$10.7^{+0.2}_{-0.2}$	$10.2^{+0.2}_{-0.3}$	$8.8^{+0.5}_{-0.3}$	$9.4^{+0.6}_{-0.3}$	$8.9^{+0.4}_{-0.5}$
186.87/193.51	$10.1^{+0.2}_{-0.2}$	$10.5^{+0.2}_{-0.2}$	$10.0^{+0.2}_{-0.2}$	$9.1^{+0.5}_{-0.3}$	$9.5^{+0.5}_{-0.3}$	$9.0^{+0.3}_{-0.5}$
186.87/195.12	$10.1^{+0.2}_{-0.2}$	$10.5^{+0.2}_{-0.2}$	$9.9^{+0.3}_{-0.2}$	$9.3^{+0.3}_{-0.4}$	$9.5^{+0.3}_{-0.5}$	$8.9^{+0.3}_{-0.4}$
196.64/192.39	$9.9^{+0.2}_{-0.3}$	$10.9^{+0.2}_{-0.2}$	$10.4^{+0.2}_{-0.4}$			
196.64/193.51	$10.0^{+0.2}_{-0.3}$	$10.7^{+0.2}_{-0.2}$	$10.2^{+0.3}_{-0.3}$			
196.64/195.12	$10.0^{+0.3}_{-0.3}$	$10.7^{+0.2}_{-0.3}$	$10.1^{+0.3}_{-0.4}$			

incorrectly identified the 186.854 Å line as due to S XI). The agreement between the 3–39 (186.887 Å) and 3–34 (196.640 Å) lines is excellent, indicating a log N_e = 8.9 cm^{-3}, a much lower value compared to what is obtained if the Binello et al. (1998a,b) data are used (see Binello et al. 2001, for an extensive discussion).

On the other hand, the 2–36 (186.854 Å) line seems to be slightly blended. Note, however, that the intensity of the 2–36 line is half of the 3–39 (186.887 Å) one. Therefore, in medium-resolution spectra, this possible blend would only provide a small contribution to the total intensity of the observed line. Indeed, in the Malinovsky & Heroux (1973) spectrum (see Fig. 8), this line indicates a log N_e = 8.8 cm^{-3}, in excellent agreement with the electron densities derived from other ions (see Del Zanna et al. 2004, for Fe X), and in stark contrast to the results obtained with the use of the Binello et al. (1998a,b) data (see Binello et al. 2001).

A similar situation occur for the SERTS-95 spectra. As shown in Table 9, the electron densities obtained with the present data are much lower than those obtained with the Binello et al. (1998a,b) data.

At longer wavelengths, the 3–10 (338.264 Å) transition is also a good density diagnostic for the solar corona. Figure 9 shows that with the present atomic data a density log N_e = 9.2 cm^{-3} is obtained from the Behring et al. (1976) observation, a value much lower than those previously obtained with the Flower (1977) and Binello et al. (1998a,b) data. Note that a log N_e = 9.2 cm^{-3} value is in broad agreement with what we derived from the lines observed at ≃190 Å (log N_e = 8.9 cm^{-3}). A 20% contribution from an unknown blend would bring agreement. However this is well within the uncertainty in the measurement. The possibility of a small blend is also suggested by the calibrated SERTS-89 data, as shown in Fig. 10. The present results indicate a log N_e = 9.8 cm^{-3}, to be compared to the value of log N_e = 9.5 cm^{-3}, obtained by the use of other ions (see Young et al. 1998).

A more definitive assessment will only be possible once the atomic data for the other ions are also checked. However, our results provide, within the uncertainties, and for various solar observations, electron densities in broad agreement with those obtained from other ions, while the previous calculations from Flower (1977) and Binello et al. (1998a,b) provided much higher values.

5. Summary and conclusions

A new calculation of rates for electron collisional excitation of Fe XII has been described which set out to remedy the perceived shortcomings of the most recent and elaborate work on this ion (Binello et al. 1998a,b, 2001). Although we have used the same basis set to describe the target for the collision process as these authors, the target itself was enlarged to include all the states of the $3s3p^33d$ configuration and some states of $3s^23p3d^2$. We have shown that additional resonance processes are introduced by this extension which significantly increase the collision strengths at low energies, particularly for transitions between the ground $3s^23p^3$ configuration and the first excited even parity configuration $3s3p^4$. These enhancements lead to increases in the thermally averaged collision strengths, particularly at lower temperatures.

We have also shown that rates for collisional processes from the ground level $3s^23p^3\ ^4S^o_{3/2}$ to other levels of the ground configuration have previously been underestimated due to the method that was used to transform the collisional data into intermediate coupling. Additional resonance effects which were not correctly treated previously are introduced by the use of the intermediate coupling frame transformation method. We have also shown that there is excellent agreement between the ICFT method and a full Breit-Pauli calculation, strongly indicating that the ICFT results are to be preferred over any previous work. As a result, the relative populations of the four excited levels of the ground configuration are significantly larger than those derived from any previous set of atomic data.

We have compared our predicted line intensities for a selection of important EUV Fe XII lines, observed in the 180–200 and 330–370 Å ranges against various observations. For the density-insensitive lines, we find excellent agreement between observation and theory. The density-sensitive lines, in addition, provide electron densities that are, within the uncertainties, in good agreement with those derived from other ions of comparable ionization potential.

We have demonstrated, with examples, the various limitations of the previous calculations, and resolved a few long-standing problems. Some minor refinements in terms of line blending still need to be addressed, however we believe that the present collisional dataset can reliably be used for plasma diagnostic in a wide range of astrophysical sources.

Acknowledgements. Support from PPARC is acknowledged. P.J.S. would like to acknowledge the support of the Université Paris 7 and the hospitality of the Observatoire de Paris.

References

Behring, W. E., Cohen, L., Doschek, G. A., & Feldman, U. 1976, ApJ, 203, 521
Binello, A. M., Landi, E., Mason, H. E., Storey, P. J., & Brosius, J. W. 2001, A&A, 370, 1071
Binello, A. M., Mason, H. E., & Storey, P. J. 1998a, A&AS, 127, 545
Binello, A. M., Mason, H. E., & Storey, P. J. 1998b, A&AS, 131, 153
Brosius, J. W., Davila, J. M., & Thomas, R. J. 1998a, ApJ, 497, L113
Brosius, J. W., Davila, J. M., & Thomas, R. J. 1998b, ApJS, 119, 255
Burgess, A. 1974, JPhB, 7, L364
Burgess, A., & Tully, J. A. 1992, A&A, 254, 436
Corliss, C., & Sugar, J. 1982, JPCRD, 11, 135
Del Zanna, G., Berrington, K., & Mason, H. E. 2004, A&A, 422, 731
Del Zanna, G., & Mason, H. E. 2005, A&A, 433, 731
Eissner, W., Jones, M., & Nussbaumer, H. 1974, CoPhC, 8, 270
Flower, D. R. 1977, A&A, 54, 163
Griffin, D. C., Badnell, N. R., & Pindzola, M. S. 1998, JPhB, 31, 3713
Hummer, D. G., Berrington, K. A., Eissner, W., et al. 1993, A&A, 279, 298
Jupen, C., Isler, R. C., & Trabert, E. 1993, MNRAS, 264, 627
Landman, D. A. 1978, ApJ, 220, 366
Malinovsky, L., & Heroux, M. 1973, ApJ, 181, 1009
Mason, H. E. 1994, ADNDT, 57, 305
Nussbaumer, H., & Storey, P. J. 1978, A&A, 64, 139
Saraph, H. E. 1978, CoPhC, 15, 247
Saraph, H. E., & Storey, P. J. 1996, A&AS, 115, 151
Storey, P. J., Mason, H. E., & Young, P. R. 2000, A&AS, 141, 285
Storey, P. J., & Zeippen, C. J. 2001, MNRAS, 324, L7
Storey, P. J., Zeippen, C. J., & Le Dourneuf, M. 2002, A&A, 394, 753
Tayal, S. S., & Henry, R. J. W. 1988, ApJ, 329, 1023
Tayal, S. S., Henry, R. J. W., & Pradhan, A. K. 1987, ApJ, 319, 951
Thomas, R. J., & Neupert, W. M. 1994, ApJS, 91, 461
Young, P. R., Landi, E., & Thomas, R. J. 1998, A&A, 329, 291
Zhitnik, I. A., Kuzin, S. V., Oraevskii, V. N., et al. 1998, AstL, 24, 819